THE JOURNAL OF PHYSICAL CHEMISTRY C

Article

Cite This: J. Phys. Chem. C XXXX, XXX, XXX−XXX

pubs.acs.org/JPCC

Ligand Effect on the Electronic Structure of Cobalt Sulfide Clusters: A Combined Experimental and Theoretical Study

Gaoxiang Liu,[†] Vikas Chauhan,[‡] Alexander P. Aydt,[§] Sandra M. Ciborowski,[†] Andrew Pinkard,[§] Zhaoguo Zhu,[†] Xavier Roy,*[,§] Shiv N. Khanna,*[,‡] and Kit H. Bowen*[,†]

[†]Department of Chemistry, Johns Hopkins University, Baltimore, Maryland 21218, United States

[‡]Department of Physics, Virginia Commonwealth University, 701 West Grace Street, Richmond, Virginia 23284, United States

[§]Department of Chemistry, Columbia University, New York, New York 10027, United States

Supporting Information

ABSTRACT: Recent studies have shown that capping ligands offer a new dimension for fine-tuning the properties of clusters. Here we investigate this concept by measuring the anion photoelectron spectra of a series of hexanuclear cobalt sulfide clusters, Co_6S_8, passivated by different numbers of triethylphosphine ligands, PEt_3. We find that the addition of PEt_3 gradually shifts the electronic spectrum of the cluster to higher energy, leading to a decrease in its electron affinity. Density functional theory calculations reveal that adding ligands demagnetizes the Co_6S_8 core. The decrease in electron affinity results from a monotonic increase in the energy of the cluster lowest unoccupied molecular orbitals (LUMO). This effect is attributed to the electron donation from the ligands to the cluster core, which increases the charge density in the core region.

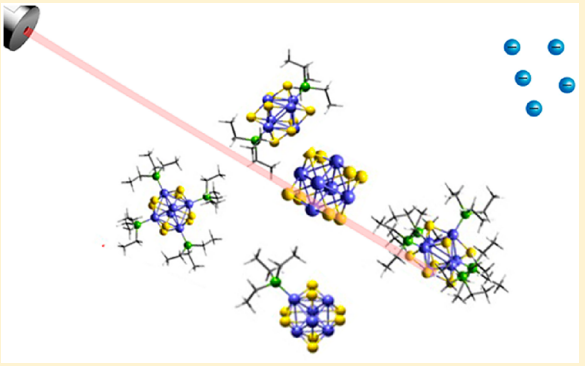

INTRODUCTION

Quantum confinement in small symmetric clusters can result in a grouping of electronic states into shells, leading to the formation of stable clusters with a well-defined valence. The resemblance to atomic shells has prompted the description of such entities as superatoms.[1] Utilizing these clusters as the "superatomic" building blocks for the assembly of novel materials represents a frontier in material science.[1−22] Within this context, the family of metal chalcogenide molecular clusters has recently received renewed attention for fabricating functional materials with tunable properties including ferromagnetism, electrical conductivity, optical gaps, and thermal conductivity switching.[2,7,23−32] One of the key advantages of such materials over traditional atomic solids is that the properties of the superatomic building blocks can be tailored preassembly. While the composition and structure of the cluster are traditionally used to control the behavior of the superatomic building unit, the capping ligands have recently received attention as valuable knobs for fine-tuning.[33,34] Capping ligands can modulate the electronic characteristics of the cluster core and direct the assembly into solid state materials.

Recently, Khanna and co-workers theoretically predicted a variety of properties that can be tuned by modifying the capping ligands of metal chalcogenide clusters. Using $Co_6Te_8L_6$ (L = capping ligand) as a model system, they have shown that changing L from PEt_3 to CO increases the electron affinity of the cluster, in effect transforming it from a superatomic alkali metal to a superatomic halogen.[14] Such an ability to alter the donor/acceptor behavior of the building blocks offers unique opportunity for creating materials with fine-tuned properties.[34] In a related study, it was predicted that the ionization energy of the Co_6Se_8 cluster can be gradually decreased by sequentially coordinating PEt_3 capping ligands to its surface metal atoms.[35] Binding carbon monoxide (CO) ligands to the Co_6Se_8 cluster, however, results in the gradual demagnetization of the core, thus stabilizing it.[36] Experimentally demonstrating these predictions by measuring the electronic structures of metal chalcogenide clusters is challenging, however, because it requires bringing the charged clusters with a controlled number of ligands into the gas phase without damaging the inorganic core. Common ionization methods (e.g., electrospray ionization and matrix-assisted laser desorption/ionization) fail to generate the desirable anions in the gas phase due to the effect of the solvent/matrix on charged clusters: the obtained anions are either dehydrogenated or tagged by the solvent/matrix molecules.

We recently reported an experimental study supported by theoretical calculations establishing the tunability of the electronic properties of the cluster $Co_6S_8(PEt_3)_{6-n}(CO)_n$ by altering the ligand ratio.[38] The unique infrared desorption/laser photoemission (IR/PE) supersonic expansion source

Received: May 2, 2019
Revised: September 13, 2019
Published: September 20, 2019

DOI: 10.1021/acs.jpcc.9b04153
J. Phys. Chem. C XXXX, XXX, XXX−XXX

used in that work serves as the ideal tool to bring the cluster into the gas phase with different number of ligands while maintaining the core structure. Here, we employ this method to investigate a series of cobalt sulfide clusters passivated with varying numbers of PEt_3 ligands. The cluster $Co_6S_8(PEt_3)_6$ is synthesized and then brought into the gas phase, where ligands are sequentially dissociated and electrons are attached to form anions, using the IR/PE source. Mass spectrometry confirms the existence of $Co_6S_8(PEt_3)_x^-$ with x ranging from 0 to 6. We find that the electron affinity and vertical detachment energy decrease with increasing ligation, demonstrating the electronic spectral tunability of this family of superatoms.

METHODS

Synthesis. Dicobalt octacarbonyl and sulfur were purchased from Strem Chemicals. PEt_3 was obtained from Alfa Aesar. All other reagents and solvents were purchased from Sigma-Aldrich. Dry and deoxygenated solvents were prepared by elution through a dual-column solvent system (MBraun). Unless otherwise stated, all reactions and sample preparations were carried out under inert atmosphere using standard Schlenk techniques or in a N_2-filled glovebox. While a multistep synthesis of $Co_6S_8(PEt_3)_6$ has been previously reported,[37] we have developed an alternative one-pot approach detailed below.[38]

$Co_6S_8(PEt_3)_6$. Sulfur (1.16 g, 36.25 mmol) was suspended in 30 mL of toluene in a 200 mL Schlenk flask. In two separate flasks, $Co_2(CO)_8$ (4.12 g, 12.05 mmol) and PEt_3 (4.27 g, 36.14 mmol) were dissolved in 20 mL of toluene. The $Co_2(CO)_8$ solution was added to the S suspension, followed by quick addition of the PEt_3 solution. The reaction mixture was refluxed under N_2 for 2 days. The reaction mixture was then opened to air, and hot filtered through Celite. The filtrate was cooled to room temperature and left to stand for ~3 h. Black crystals formed during that period; the resulting suspension was filtered through a fine frit, and the solid was washed with toluene and diethyl ether. The dark, black crystals were collected, dried *in vacuo*, and stored under N_2. Yield: 2.2 g (42%). The characterization data are as previously published. MS-MALDI m/z^+ calculated 1317.92; found, 1317.95.

Anion Photoelectron Spectroscopy. Anion photoelectron spectroscopy was conducted by crossing a mass-selected negative ion beam with a fixed energy photon beam and analyzing the energies of the resultant photodetached electrons. This technique is governed by the well-known energy-conserving relationship, $h\nu$ = EBE + EKE, where $h\nu$, EBE, and EKE are the photon energy, electron binding energy (photodetachment transition energy), and the electron kinetic energy, respectively. The details of our apparatus have been described elsewhere.[39,40] Briefly, the photoelectron spectra were collected on an apparatus consisting of an ion source, a linear time-of-flight mass spectrometer for mass analysis and selection, and a magnetic-bottle photoelectron spectrometer for electron energy analysis (resolution ~35 meV at 1 eV EKE). The third harmonic (355 nm, 3.49 eV per photon) of a Nd:YAG was used to photodetach electrons from the cluster anion of interest. Photoelectron spectra were calibrated against the well-known atomic lines of the copper anion, Cu^-.

To make $Co_6S_8(PEt_3)_x^-$ in the gas phase, a specialized infrared desorption/laser photoemission (IR/PE) supersonic helium expansion source was employed.[38,41] Briefly, a low power IR pulse (1064 nm) from a Nd:YAG laser hit a translating graphite bar thinly coated with the $Co_6S_8(PEt_3)_6$ sample. Because the graphite absorbed most of the energy, a localized thermal shock lasting a few nanoseconds propelled the clusters into the gas phase. Almost simultaneously, a high power pulse of 532 nm light from a second Nd:YAG laser struck a close-by photoemitter (Hf wire), creating a shower of electrons that attached to the evaporated neutral clusters. Also, almost simultaneously, a plume of ultrahigh purity helium gas rapidly expanded from a pulsed valve located slightly upstream, cooling the nascent anions and directing them into the mass spectrometer, where they were analyzed. The $Co_6S_8(PEt_3)_6$ cluster was coated onto a graphite bar in a N_2-filled glovebox, which was then enclosed inside an airtight "suitcase" container and opened under high vacuum after being transferred to the vacuum chamber.

Theoretical Calculations. Electronic structure modeling of the anion and neutral $Co_6S_8(PEt_3)_x$ (x = 1−5) were carried out to understand the variation in the adiabatic and vertical detachment energies at the microscopic level. The exchange-correlation effects are included via a generalized gradient functional PBE detailed by Perdew et al.[42] The cluster wave function is formed from a linear combination of atomic orbitals constructed from Slater-type orbitals located on the atomic sites.[43] A TZ2P basis set and a large frozen electron core (S: $1s^2 2s^2 p^6$, Co: $1s^2 2s^2 p^6 3s^2 p^6$, P: $1s^2 2s^2 p^6$, C: $1s^2$) are used. The calculations incorporate a zero-order regular approximation (ZORA) to include scalar-relativistic effect.[44,45] The trial structures of the clusters are taken from the previously optimized structure of the $Co_6Se_8(PEt_3)_x$ where the Se sites are replaced by S. A quasi-Newton method without any symmetry restriction allowed a determination of the ground state of the clusters. During optimization, we investigated all possible spin states. Also, none of the clusters in their ground states has the spin-contamination. The adiabatic electron affinity (AEA) is calculated as the difference between the total energy between the anion in its ground state geometry and the neutral cluster in its ground state geometry, while the vertical detachment energy (VDE) is given by the total energy difference between the anion in its ground state and the neutral cluster in the geometry of the anion.

RESULTS AND DISCUSSION

Figure 1 presents a typical mass spectrum of $Co_6S_8(PEt_3)_x^-$ obtained with the IR/PE source. The ultrashort thermal shock induced by IR laser irradiation caused the sequential dissociation of the PEt_3 ligand during the vaporization of the solid $Co_6S_8(PEt_3)_6$ sample into gas phase. $Co_6S_8(PEt_3)_x^-$ with x ranging from 0 to 6 was generated and investigated by anion photoelectron spectroscopy.

Figure 2 presents the anion photoelectron spectra of $Co_6S_8(PEt_3)_x^-$ (x = 2−5) collected with a 355 nm (3.49 eV) third harmonic laser. The spectrum of $Co_6S_8(PEt_3)_6^-$ has been published in a previous report.[38] Our attempts to measure the photoelectron spectra of $Co_6S_8^-$ and $Co_6S_8(PEt_3)^-$ (x = 0 and 1) with a 355 nm laser were for the most part unsuccessful: for $Co_6S_8^-$, no photoelectron signal was observed, i.e., its AEA and VDE are above 3.49 eV, while for $Co_6S_8(PEt_3)^-$, only a small portion of its spectrum could be collected because the majority of its photoelectron spectrum lies beyond the photon energy (Figure S1). The AEA and VDE of each cluster are determined from the photoelectron spectra. The value of AEA is taken to be the onset of the lowest electron binding energy (EBE) peak in the photoelectron spectrum. The VDE is the vertical transition energy from the ground state of the anion to the

DOI: 10.1021/acs.jpcc.9b04153
J. Phys. Chem. C XXXX, XXX, XXX−XXX

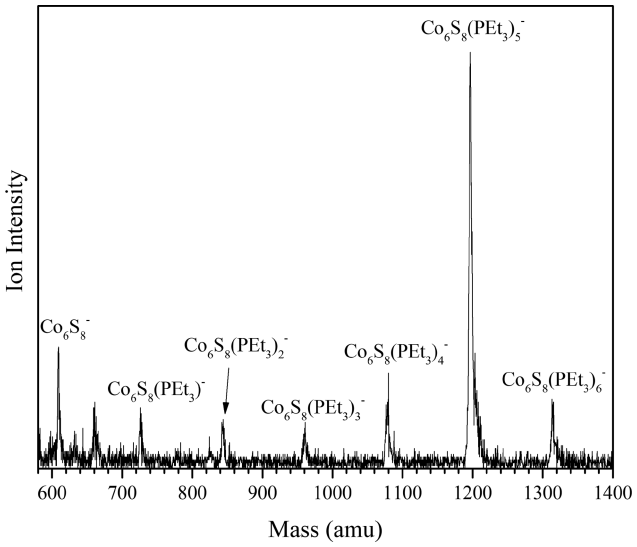

Figure 1. Anion mass spectrum of $Co_6S_8(PEt_3)_x^-$ generated using IR/PE anion source.

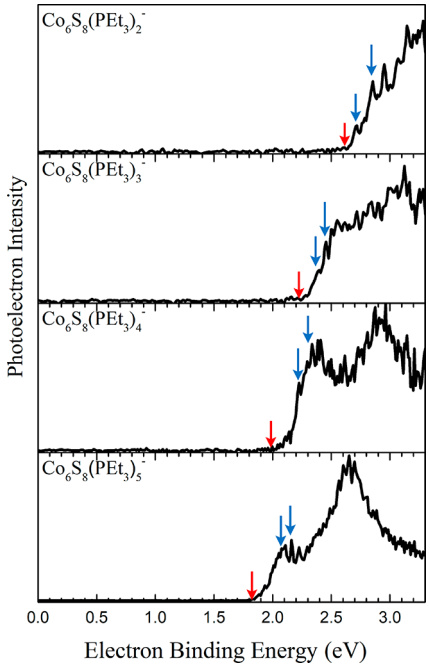

Figure 2. Negative ion photoelectron spectra of $Co_6S_8(PEt_3)_x^-$ (x = 2−5) anions collected using 355 nm (3.49 eV) photons from a Nd:YAG laser. The red arrows indicate the AEA, the blue arrows indicate the VDE and the VDE*.

neutral ground electronic state at the anion geometry. It is determined as the EBE value at the intensity maximum of the peak of interest. Here, however, because of the large number of electronic states that can be accessed during the photodetachment process, the photoelectron spectra are convoluted. We therefore determine the VDE as the EBE of the first noticeable peak in each spectrum. Based on the anion photoelectron spectra, the AEA values of $Co_6S_8(PEt_3)_x$ are 3.0, 2.6, 2.2, 2.0, and 1.8 eV for x = 1, 2, 3, 4, and 5, respectively, while the corresponding anion VDE values are 3.22, 2.71, 2.44, 2.31, and 2.05 eV, respectively. We also report the VDE* values, which correspond to the transition from the anion ground state to the first electronic excited state of the neutral, as the EBE of the second noticeable peak. Their values are 3.35, 2.85, 2.45. 2.29, and 2.16 eV for x = 1, 2, 3, 4, and 5, respectively. By sequentially adding PEt_3 ligands to the Co_6S_8 core, the AEA and VDE of this superatom decrease systematically, which is consistent with the electron-donating nature of the PEt_3 ligands.

Changes in the electronic properties of the cluster are evident in high energy spectral features above the first EBE peak. These higher EBE peaks arise from transitions from the anion ground state to excited electronic states of the neutral cluster, and the shape of these features relates to the electronic structure of the neutral clusters. As x increases, the photoelectron spectra of $Co_6S_8(PEt_3)_x^-$ shifts to lower electron binding energy, and the overall spectral shapes change significantly. Such observation suggests a change in the electronic structure of $Co_6S_8(PEt_3)_x^-$ as x changes. Note that this is different from the previous study of $Co_6S_8(PEt_3)_{6-n}(CO)_n^-$ where the photoelectron spectra shift to higher electron binding energy as the CO ratio increases, but the overall spectral shapes are maintained, indicating that the essential electronic structure of $Co_6S_8(PEt_3)_{6-n}(CO)_n$ superatoms are largely unchanged.[38]

The structures of the anionic and neutral $Co_6S_8(PEt_3)_x$ clusters were investigated by theoretical calculations. Figure 3

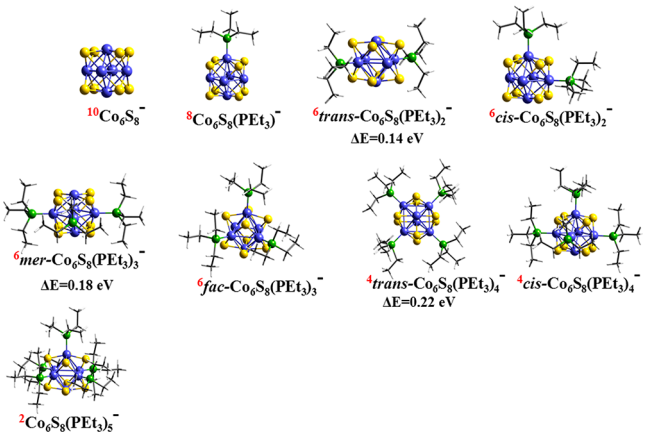

Figure 3. Optimized ground state geometry of anionic $Co_6S_8(PEt_3)_x$ (x = 0−5) clusters. Superscripts in red text show the multiplicity of the clusters.

shows the optimized ground state geometries of $Co_6S_8(PEt_3)_x^-$, while those of the neutral species are in Figure S2. For x = 2 and x = 4, the clusters can either be *cis* or *trans* isomers. In both cases, the *trans* isomers are higher in energy, by ∼0.14 and ∼0.22 eV, respectively. A similar situation arises for the corresponding neutral clusters: the *trans* isomers are ∼0.01 and ∼0.25 eV higher in energy for x = 2 and x = 4, respectively. For $Co_6S_8(PEt_3)_3$, the cluster can adopt *fac* and *mer* configurations. We find that the *fac* isomer is the ground state for both anionic and neutral clusters, being lower in energy by ∼0.18 and ∼0.04 eV, respectively. In addition to the ligated clusters, we optimize the anionic and neutral naked Co_6S_8 core in order to complete the analysis, although no photoelectron spectrum could be measured as the transitions are outside the range of measurable energies.

The key experimental finding in Figure 2 is that the bonding of PEt_3 to the Co_6S_8 core leads to a change in the peak position and the leading edge of the spectrum. To provide insight into these variations, we calculate the VDE by taking the energy

DOI: 10.1021/acs.jpcc.9b04153
J. Phys. Chem. C XXXX, XXX, XXX−XXX

difference between the ground state of the anion and neutral cluster with the same geometry as the anion. The VDE corresponds to the first peak maximum in the photodetachment spectra and provides the most direct comparison with the experiment, while an estimation of the second VDE is obtained by a vertical transition from the anion ground state to the neutral with next higher spin multiplicity. We also calculated the AEA, which are determined by the onset of the experimental spectra and corresponds to the energy difference between the ground states of the anion and neutral species. Finally, we examine the excited states of the neutral cluster in the anionic geometry that correspond to the spectral features beyond the first peak. Figure 4 compares the experimental and

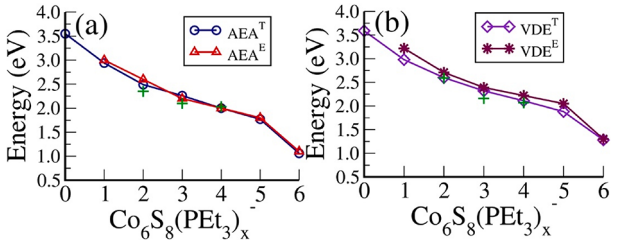

Figure 4. Experimental and theoretical adiabatic and vertical detachment energy of $Co_6S_8(PEt_3)_x$ (x = 0–6) clusters. The plus symbol (+) indicates the AEA^T and VDE^T values of the cluster's isomers at x = 2, 3, and 5. The results of $Co_6S_8(PEt_3)_6$ are taken from ref 38.

theoretical AEA and VDE values, while Table 1 lists the values of both the theoretical and calculated AEA and VDE. The calculated AEA and VDE of the Co_6S_8 core are 3.55 and 3.59 eV, respectively, which are in accordance with the absence of photoelectron signal when using 355 nm (3.49 eV) photon. The AEA^T for $Co_6S_8(PEt_3)$ is 2.94 eV, agreeing with the AEA^E of 3.0 eV, while VDE^E is 3.22 eV compared to the calculated VDE^T of 2.98 eV. The *cis*-$Co_6S_8(PEt_3)_2$ isomer has an AEA^T of 2.49 eV, which is slightly closer to the AEA^E of 2.6 eV than that of *trans*-$Co_6S_8(PEt_3)_2$ (2.35 eV). Both $Co_6S_8(PEt_3)_2$ isomers have VDE^T around 2.60 eV that are close to the VDE^E of 2.71 eV, suggesting the possible presence of both isomers. The AEA^T and VDE^T of *fac*-$Co_6S_8(PEt_3)_3$ are 2.26 and 2.32 eV, in very good agreement with corresponding experimental values of AEA^E (2.2 eV) and VDE^E (2.39 eV), while the AEA^T and VDE^T for *mer*-$Co_6S_8(PEt_3)_3$ are 2.10 and 2.16 eV. Both *trans*- and *cis*-$Co_6S_8(PEt_3)_4$ have AEA^T around 2.0 eV, matching the experimental value of 2.0 eV, while the corresponding VDE^T (2.15 and 2.11 eV) values are slightly smaller than the experimental value of 2.31 eV. In order to evaluate the dispersion effect on the calculated AEA^T and VDE^T, we also carried out calculations with Grimme dispersion corrected PBE functional.[46] Similar calculated AEA^T and VDE^T were obtained (Table S1). Overall, the calculated values are in excellent agreement with experimental results, thus validating the calculations. Since the photoelectron spectra are fingerprints of the electronic structures of neutral clusters, the agreement indicates that the calculated atomic structures and the multiplicities match the ones observed experimentally.

The main result is a monotonic decrease in the AEA and VDE as ligands are successively attached to the Co_6S_8 core. Such a decrease is attributed to the fact that PEt_3 ligands are electron donors and thus increase the charge density in the core region. To support this hypothesis, we performed a Hirshfeld charge analysis (Figure S3). The cumulative charge donated from the ligands to the Co_6S_8 core gradually increases, from ~0.32 e in $Co_6S_8(PEt_3)$ to ~0.90 e in $Co_6S_8(PEt_3)_5$. The added charge affects the one-electron levels of the clusters, in particular, the HOMO and LUMO energies, which control the ionization and electron affinity. Figure 5 presents the one-electron levels of the neutral clusters. The values of the HOMO, LUMO, and HOMO–LUMO gap for anionic and neutral clusters are given in Table S2. Note that the addition of successive ligands raises the one-electron levels, as marked by the position of the LUMO. As the position of the LUMO is raised in energy, the electron affinity of the cluster decreases since the extra electron occupies the LUMO of the neutral cluster. The largest increase in the LUMO energy occurs with the attachment of the first and second PEt_3. Beyond x = 2, each additional ligand increases the LUMO by around 0.3 eV. Remarkably, we find that the ligands are not bound strongly to the cluster core: the binding energy of the first PEt_3 to Co_6S_8 is 1.53 eV and decreases to 1.38 eV for the fifth ligand.

Our earlier studies have shown that a complete ligation with either PEt_3 or a mixture of PEt_3 and CO ligands produces the lowest spin state for the $Co_6S_8(PEt_3)_{6-n}(CO)_n$ clusters. This contrasts drastically with the partially ligated cluster in this study: starting from the bare anionic Co_6S_8 core, with a spin multiplicity of M = 10, the multiplicity is reduced by 2 upon the addition of a PEt_3 ligand, leading to $Co_6S_8(PEt_3)^-$ in an octet state. The attachment of the second and third PEt_3 ligands produces a sextet spin state, while the bonding of the fourth and fifth ligands generates a quartet ground state. To support these results, Figure 6a shows the one-electron energy levels of Co_6S_8 in an octahedral symmetry. In the energy range

Table 1. Theoretical and Experimental Adiabatic and First and Second Vertical Detachment Energies (VDE and VDE*) of $Co_6S_8(PEt_3)_x^-$ (x = 0–5) Clusters

		VDE^E (eV)					VDE^T (eV)	
cluster	AEA^E (eV)	VDE	VDE*	isomers	ΔE (eV)	AEA^T (eV)	VDE	VDE*
$Co_6S_8^-$	>3.49	>3.49	>3.49			3.55	3.59	3.96
$Co_6S_8(PEt_3)^-$	3.0	3.22	3.35			2.94	2.98	3.37
$Co_6S_8(PEt_3)_2^-$	2.6	2.71	2.85	*trans*	0.14	2.35	2.59	2.88
				cis		2.49	2.60	2.92
$Co_6S_8(PEt_3)_3^-$	2.2	2.39	2.45	*mer*	0.18	2.10	2.16	2.32
				fac		2.26	2.32	2.33
$Co_6S_8(PEt_3)_4^-$	2.0	2.22	2.29	*trans*	0.22	2.03	2.07	2.15
				cis		2.00	2.11	2.21
$Co_6S_8(PEt_3)_5^-$	1.8	2.05	2.16			1.77	1.88	2.09

DOI: 10.1021/acs.jpcc.9b04153
J. Phys. Chem. C XXXX, XXX, XXX–XXX

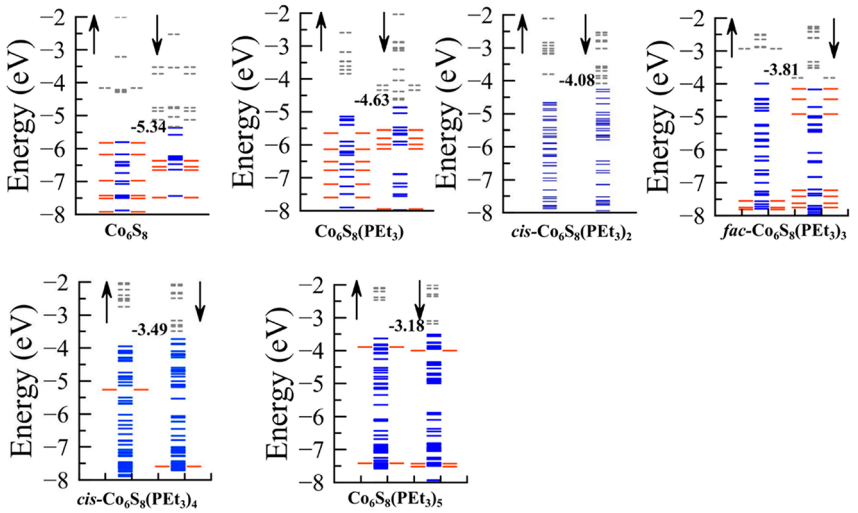

Figure 5. One-electron energy levels of $Co_6S_8(PEt_3)_x$ (x = 0−5) clusters. The solid blue and red bars represent the singly and doubly occupied energy levels, respectively. Unoccupied energy levels are shown by dashed gray lines. The energy of LUMO (in eV) is indicated for each cluster. The α-spin and β-spin channel are represented by up and down arrows.

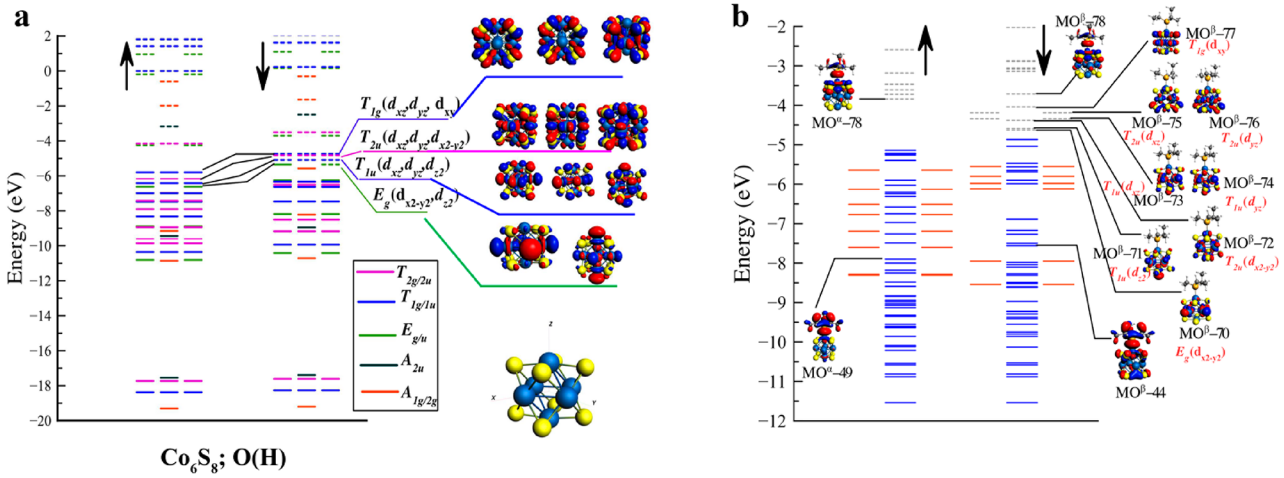

Figure 6. (a) One-electron energy levels with their symmetry labels for Co_6S_8 in octahedron symmetry. The solid and dashes lines represent occupied and unoccupied energy levels. (b) One-electron energy levels along with their iso-surfaces for $Co_6S_8(PEt_3)$. The solid blue and red bars represent the singly and doubly occupied energy levels, respectively. Unoccupied energy levels are shown by dashed gray lines. The α-spin and β-spin channels are represented by up and down arrows.

−20 to −18 eV, there are 16 electrons accommodated in A_{1g}, T_{1u}, T_{2g}, and A_{2u} orbitals formed by *s*-states of S and Co sites. The remaining 86 electrons are accommodated in $T_{2g/2u}$, T_{1g}/T_{1u}, $E_{g/u}$, A_{2u}, and $A_{1g/2g}$ states in the energy range from −10 to −2 eV. A set of unoccupied T_{1g} (d_{xz}, d_{yz}, d_{xy}), T_{2u} (d_{xz}, d_{yz}, $d_{x^2-y^2}$), T_{1u} (d_{xz}, d_{yz}, d_{z^2}), and E_g (d_{z^2}) states in β-spin channel lead to a spin multiplicity M = 11. In addition, the E_g ($d_{x^2-y^2}$) in the β-spin channel is occupied. As the LUMO is a minority spin state, addition of an electron leads to an anion with a spin multiplicity of 10. The *d*-orbitals in the parentheses with italic text are localized on the Co site along the *z*-axis. Note that two d_{z^2} orbitals form a bonding E_g-type and an antibonding T_{1u}-type orbitals with a node along *z* axis. Figure 6b shows the one-electron energy levels of Co_6S_8 with PEt_3 ligand along the *z*-axis. Addition of PEt_3 ligand breaks the octahedral symmetry, and the *sp*-states of P combine primarily with *d*-states of Co to stabilize the E_g (d_{z^2}) and T_{1g} (d_{xz}, d_{yz}) states, while the E_g ($d_{x^2-y^2}$) state is destabilized and becomes a part (MO^{β}-70) of the unoccupied states in the β-spin channel. The E_g (d_{z^2}) states form the occupied bonding (MO^{α}-49, MO^{β}-44) states with a lone pair of electrons of PEt_3, while the corresponding unoccupied antibonding (MO^{α}-78, MO^{β}-78) states are higher in energy. The remaining T_{2u} (d_{xz}, d_{yz}, $d_{x^2-y^2}$) and T_{1u} (d_{xz}, d_{yz}, d_{z^2}) also lose their degeneracy and turn into MO^{β}-(75,76,72) and MO^{β}-(73,74,71), respectively. These six states along with MO^{β}-70 and MO^{β}-77 ($T_{1g}(d_{xy})$) lead to a reduced multiplicity M = 9 in the ground state of $Co_6S_8(PEt_3)$. Further addition of ligands leads to a similar mixing with reduction in multiplicity.

SUMMARY

By combining inorganic cluster synthesis, gas-phase anion photoelectron spectroscopy, and electronic structure calculations, we have demonstrated that the electronic properties of metal chalcogenide clusters can be tuned by varying the number of phosphine capping ligands. The sequential addition of PEt_3 to the Co_6S_8 core results in a gradual decrease of its electron affinity and a shift of its electronic spectrum to lower

DOI: 10.1021/acs.jpcc.9b04153
J. Phys. Chem. C XXXX, XXX, XXX−XXX

energy. Density functional theory calculations reveal that addition of PEt_3 ligands gradually demagnetizes the Co_6S_8 core and increases its charge density. These effects stabilize the core and lift the energy of the LUMO.

■ ASSOCIATED CONTENT

Supporting Information

The Supporting Information is available free of charge on the ACS Publications website at DOI: 10.1021/acs.jpcc.9b04153.

Figures S1−S3, Tables S1−S5, and Cartesian coordinates of optimized anionic $Co_6S_8(PEt_3)_x$ (x = 0−5) clusters (PDF)

■ AUTHOR INFORMATION

Corresponding Authors

*(X.R.) E-mail: xr2114@columbia.edu.
*(S.N.K.) E-mail: snkhanna@vcu.edu.
*(K.H.B.) E-mail: kbowen@jhu.edu.

ORCID

Gaoxiang Liu: 0000-0002-1001-0064
Sandra M. Ciborowski: 0000-0001-9453-4764
Xavier Roy: 0000-0002-8850-0725
Shiv N. Khanna: 0000-0002-9797-1289
Kit H. Bowen: 0000-0002-2858-6352

Notes

The authors declare no competing financial interest.

■ ACKNOWLEDGMENTS

The gas-phase work is based on work supported by the Office of Naval Research (ONR), Multidisciplinary University Research Initiative (MURI) under Grant No. N00014-15-1-2681 (to K.H.B.), and by the Air Force Office of Scientific Research (AFOSR) under grant number FA9550-19-1-0077 (to K.H.B.). Theoretical studies (V.C. and S.N.K.) were supported by a grant from from the Department of Energy under Award Number DE-SC0006420. Synthetic work was supported by the Center for Precision Assembly of Superstratic and Superatomic Solids at Columbia University, an NSF MRSEC (DMR-1420634) (to X.R.), and by the Air Force Office of Scientific Research (AFOSR) under grant number FA9550-18-1-0020 (to X.R.).

■ REFERENCES

(1) Reber, A. C.; Khanna, S. N. Superatoms: Electronic and Geometric Effects on Reactivity. *Acc. Chem. Res.* **2017**, *50*, 255−263.
(2) Pinkard, A.; Champsaur, A. M.; Roy, X. Molecular Clusters: Nanoscale Building Blocks for Solid-State Materials. *Acc. Chem. Res.* **2018**, *51*, 919−929.
(3) Claridge, S. A.; Castleman, A. W.; Khanna, S. N.; Murray, C. B.; Sen, A.; Weiss, P. S. Dimensional Reduction: A Practical Formalism for Manipulating Solid Structures. *ACS Nano* **2009**, *3*, 244−255.
(4) Tulsky, E. G.; Long, J. R. Dimensional Reduction: A Practical Formalism for Manipulating Solid Structures. *Chem. Mater.* **2001**, *13*, 1149−1166.
(5) Baudron, S. A.; Batail, P.; Coulon, C.; Clerac, R.; Canadell, E.; Laukhin, V.; Melzi, R.; Wzietek, P.; Jerome, D.; Auban-Senzier, P.; Ravy, S. (EDT-TTF-$CONH_2$)$_6$[$Re_6Se_8(CN)_6$], a Metallic Kagome-Type Organic−Inorganic Hybrid Compound: Electronic Instability, Molecular Motion, and Charge Localization. *J. Am. Chem. Soc.* **2005**, *127*, 11785−11797.
(6) Yoon, B.; Luedtke, W. D.; Barnett, R. N.; Gao, J.; Desireddy, A.; Conn, B. E.; Bigioni, T.; Landman, U. Hydrogen-bonded structure and mechanical chiral response of a silver nanoparticle superlattice. *Nat. Mater.* **2014**, *13*, 807−811.
(7) Corrigan, J. F.; Fuhr, O.; Fenske, D. Metal Chalcogenide Clusters on the Border between Molecules and Materials. *Adv. Mater.* **2009**, *21*, 1867−1871.
(8) Roy, X.; Lee, C. H.; Crowther, A. C.; Schenck, C. L.; Besara, T.; Lalancette, R. A.; Siegrist, T.; Stephens, P. W.; Brus, L. E.; Kim, P.; Steigerwald, M. L.; Nuckolls, C. Nanoscale Atoms in Solid-State Chemistry. *Science* **2013**, *341*, 157−160.
(9) Khanna, S. N.; Jena, P. Atomic clusters: Building Blocks for a Class of Solids. *Phys. Rev. B: Condens. Matter Mater. Phys.* **1995**, *51*, 13705−13716.
(10) Castleman, A. W.; Khanna, S. N. Clusters, Superatoms, and Building Blocks of New Materials. *J. Phys. Chem. C* **2009**, *113*, 2664−2675.
(11) Lee, C. H.; Liu, L.; Bejger, C.; Turkiewicz, A.; Goko, T.; Arguello, C. J.; Frandsen, B. A.; Cheung, S. C.; Medina, T.; Munsie, T. J. S.; D'Ortenzio, R.; Luke, G. M.; Besara, T.; Lalancette, R. A.; Siegrist, T.; Stephens, P. W.; Crowther, A. C.; Brus, L. E.; Matsuo, Y.; Nakamura, E.; Uemura, Y. L.; Kim, P.; Nuckolls, C.; Steigerwald, M. L.; Roy, X. Ferromagnetic Ordering in Superatomic Solids. *J. Am. Chem. Soc.* **2014**, *136*, 16926−16931.
(12) Roy, X.; Schenck, C. L.; Ahn, S.; Lalancette, R. A.; Venkataraman, L.; Nuckolls, C.; Steigerwald, M. L. Quantum Soldering of Individual Quantum Dots. *Angew. Chem., Int. Ed.* **2012**, *51*, 12473−12476.
(13) Trinh, M. T.; Pinkard, A.; Pun, A. B.; Sanders, S. N.; Kumarasamy, E.; Sfeir, M. Y.; Campos, L. M.; Roy, X.; Zhu, X. Y. Distinct Properties of the Triplet Pair State from Singlet Fission. *Sci. Adv.* **2017**, *3*, No. e1700241.
(14) Chauhan, V.; Reber, A. C.; Khanna, S. N. Metal Chalcogenide Clusters with Closed Electronic Shells and the Electronic Properties of Alkalis and Halogens. *J. Am. Chem. Soc.* **2017**, *139*, 1871−1877.
(15) Khanna, S. N.; Reber, A. C. Intercalation without Altercation. *Nat. Chem.* **2017**, *9*, 1151−1152.
(16) Tomalia, D. A.; Khanna, S. N. A Systematic Framework and Nanoperiodic Concept for Unifying Nanoscience: Hard/Soft Nanoelements, Superatoms, Meta-Atoms, New Emerging Properties, Periodic Property Patterns, and Predictive Mendeleev-like Nanoperiodic Tables. *Chem. Rev.* **2016**, *116*, 2705−2774.
(17) Zheng, Z.; Long, J. R.; Holm, R. H. A Basis Set of Re_6Se_8 Cluster Building Blocks and Demonstration of Their Linking Capability: Directed Synthesis of an $Re_{12}Se_{16}$ Dicluster. *J. Am. Chem. Soc.* **1997**, *119*, 2163−2171.
(18) Cargnello, M.; Johnston-Peck, A. C.; Diroll, B. T.; Wong, E.; Datta, B.; Damodhar, D.; Doan-Nguyen, V. V. T.; Herzing, A. A.; Kagan, C. R.; Murray, C. B. Substitutional Doping in Nanocrystal Superlattices. *Nature* **2015**, *524*, 450−453.
(19) O'Brien, M. N.; Jones, M. R.; Lee, B.; Mirkin, C. A. Anisotropic Nanoparticle Complementarity in DNA-mediated Co-crystallization. *Nat. Mater.* **2015**, *14*, 833−839.
(20) Boles, M. A.; Talapin, D. V. Many-Body Effects in Nanocrystal Superlattices: Departure from Sphere Packing Explains Stability of Binary Phases. *J. Am. Chem. Soc.* **2015**, *137*, 4494.
(21) Poyser, C. L.; Czerniuk, T.; Akimov, A.; Diroll, B. T.; Gaudling, E. A.; Salasyuk, A. S.; Kent, A. J.; Yakovlev, D. R.; Bayer, M.; Murray, C. B. Coherent Acoustic Phonons in Colloidal Semiconductor Nanocrystal Superlattices. *ACS Nano* **2016**, *10*, 1163−1169.
(22) Ong, W. L.; Rupich, S. M.; Talapin, D. V.; McGaughey, A. J. H.; Malen, J. A. Surface Chemistry Mediates Thermal Transport in Three-dimensional Nanocrystal Arrays. *Nat. Mater.* **2013**, *12*, 410−415.
(23) Voevodin, A.; Campos, L. M.; Roy, X. Multifunctional Vesicles from a Self-assembled Cluster-Containing Diblock Copolymer. *J. Am. Chem. Soc.* **2018**, *140*, 5607−5611.
(24) Champsaur, A. M.; Yu, J.; Roy, X.; Paley, D. M.; Steigerwald, M. L.; Nuckolls, C.; Bejger, C. M. Two-Dimensional Nanosheets from Redox-Active Superatoms. *ACS Cent. Sci.* **2017**, *3*, 1050−1055.

DOI: 10.1021/acs.jpcc.9b04153
J. Phys. Chem. C XXXX, XXX, XXX−XXX

(25) Champsaur, A. M.; Mézière, C.; Allain, M.; Paley, D. W.; Steigerwald, M. L.; Nuckolls, C.; Batail, P. Weaving Nanoscale Cloth through Electrostatic Templating. *J. Am. Chem. Soc.* **2017**, *139*, 11718−11721.
(26) O'Brien, E. S.; Trinh, M. T.; Kann, R. L.; Chen, J.; Elbaz, G. A.; Masurkar, A.; Atallah, T. L.; Paley, M. V.; Patel, N.; Paley, D. W.; Kymissis, I.; Crowther, A. C.; Millis, A. J.; Reichman, D. R.; Zhu, X. Y.; Roy, X. Single-crystal-to-single-crystal Intercalation of a Low-bandgap Superatomic crystal. *Nat. Chem.* **2017**, *9*, 1170−1174.
(27) Lovat, G.; Choi, B.; Paley, D. W.; Steigerwald, M. L.; Venkataraman, L.; Roy, X. Room-emperature Current Blockade in Atomically Defined Single-cluster Junctions. *Nat. Nanotechnol.* **2017**, *12*, 1050−1054.
(28) Ong, W. L.; O'Brien, E. S.; Dougherty, P. S. M.; Paley, D. W.; Fred Higgs, C., Iii; McGaughey, A. J. H.; Malen, J. A.; Roy, X. Orientational Order Controls Crystalline and Amorphous Thermal Transport in Superatomic Crystals. *Nat. Mater.* **2017**, *16*, 83−88.
(29) Choi, B.; Yu, J.; Paley, D. W.; Tuan Trinh, M.; Paley, M. V.; Karch, J. M.; Crowther, A. C.; Lee, C. H.; Lalancette, R. A.; Zhu, X.; Kim, K.; Steigerwald, M. L.; Nuckolls, C.; Roy, X. van der Waals Solids from Self-Assembled Nanoscale Building Blocks. *Nano Lett.* **2016**, *16*, 1445−1449.
(30) Champsaur, A. M.; Velian, A.; Paley, D. W.; Choi, B.; Roy, X.; Steigerwald, M. L.; Nuckolls, C. Building Diatomic and Triatomic Superatom Molecules. *Nano Lett.* **2016**, *16*, 5273−5277.
(31) Turkiewicz, A.; Paley, D. W.; Besara, T.; Elbaz, G.; Pinkard, A.; Siegrist, T.; Roy, X. Assembling Hierarchical Cluster Solids with Atomic Precision. *J. Am. Chem. Soc.* **2014**, *136*, 15873−15876.
(32) Yu, J.; Lee, C. H.; Bouilly, D.; Han, M.; Kim, P.; Steigerwald, M. L.; Roy, X.; Nuckolls, C. Patterning Superatom Dopants on Transition Metal Dichalcogenides. *Nano Lett.* **2016**, *16*, 3385−3389.
(33) Walter, M.; Akola, J.; Lopez-Acevedo, O.; Jadzinsky, P. D.; Calero, G.; Ackerson, C. J.; Whetten, R. L.; Grönbeck, H.; Häkkinen, H. A Unified View of Ligand-protected Gold Clusters as Superatom Complexes. *Proc. Natl. Acad. Sci. U. S. A.* **2008**, *105*, 9157−916.
(34) Aikens, C. M. Electronic and Geometric Structure, Optical Properties, and Excited State Behavior in Atomically Precise Thiolate-Stabilized Noble Metal Nanoclusters. *Acc. Chem. Res.* **2018**, *51*, 3065−3073.
(35) Reber, A. C.; Khanna, S. N. $Co_6Se_8(PEt_3)_6$ Superatoms as Tunable Chemical Dopants for Two-Dimensional Semiconductors. *npj Comput. Mater.* **2018**, *4*, 33.
(36) Chauhan, V.; Khanna, S. N. Strong Effect of Organic Ligands on the Electronic Structure of Metal-Chalcogenide Clusters. *J. Phys. Chem. A* **2018**, *122*, 6014−6020.
(37) Cecconi, F.; Ghilardi, C. A.; Midollini, S.; Orlandini, A. One Electron Reduction of a Cobalt-sulfur Cluster. Synthesis and Molecular Structure of $[Co_6(\mu_3\text{-}S)_8(PEt_3)_6]$·nthf. *Inorg. Chim. Acta* **1983**, *76*, 183−184.
(38) Liu, G.; Pinkard, A.; Ciborowski, S. M.; Chauhan, V.; Zhu, Z.; Aydt, A. P.; Khanna, S. N.; Roy, X.; Bowen, K. H. Tuning the Electronic Properties of Hexanuclear Cobalt Sulfide Superatoms via Ligand Substitution. *Chem. Sci.* **2019**, *10*, 1760−1766.
(39) Zhang, X.; Liu, G.; Gantefoer, G.; Bowen, K. H.; Alexandrova, A. N. $PtZnH_5^-$, A σ-Aromatic Cluster. *J. Phys. Chem. Lett.* **2014**, *5*, 1596−1601.
(40) Liu, G.; Ciborowski, S. C.; Bowen, K. Photoelectron Spectroscopic and Computational Study of PyridineLigated Gold Cluster Anions. *J. Phys. Chem. A* **2017**, *121*, 5817−5822.
(41) Grubisic, A.; Wang, H.; Li, X.; Ko, Y. J.; Kocak, S.; Pederson, M. R.; Bowen, K. H.; Eichhorn, B. W. Photoelectron Spectroscopic and Computational Studies of the $Pt@Pb_{10}^{1-}$ and $Pt@Pb_{12}^{1-/2-}$ Anions. *Proc. Natl. Acad. Sci. U. S. A.* **2011**, *108*, 14757−14762.
(42) Perdew, J. P.; Yue, W. Accurate and Simple Density Functional for the Electronic Exchange Energy: Generalized Gradient Approximation. *Phys. Rev. B: Condens. Matter Mater. Phys.* **1986**, *33*, 8800−8802.
(43) van Lenthe, E.; Baerends, E. J. Optimized Slate-type basis sets for the elements 1−118. *J. Comput. Chem.* **2003**, *24*, 1142−1156.
(44) van Lenthe, E.; van Leeuwen, R.; Baerends, E. J.; Snijders, J. G. Relativistic Regular Two-component Hamiltonians. *Int. J. Quantum Chem.* **1986**, *57*, 281−293.
(45) van Lenthe, E.; Ehlers, A.; Baerends, E. J. Geometry Optimizations in the Zero-order Regular Approximation for Relativistic Effects. *J. Chem. Phys.* **1999**, *110*, 8943−8953.
(46) Grimme, S.; Ehrlich, S.; Goerigk, L. Effect of the Damping Function in Dispersion Corrected Density Functional Theory. *J. Comput. Chem.* **2011**, *32*, 1456−1465.

DOI: 10.1021/acs.jpcc.9b04153
J. Phys. Chem. C XXXX, XXX, XXX−XXX